ARTICLES
PUBLISHED ONLINE: 6 NOVEMBER 2011 | DOI: 10.1038/NMAT3159
nature materials

# Universal energy-level alignment of molecules on metal oxides

Mark T. Greiner[1]*, Michael G. Helander[1], Wing-Man Tang[1], Zhi-Bin Wang[1], Jacky Qiu[1] and Zheng-Hong Lu[1,2]

**Transition-metal oxides improve power conversion efficiencies in organic photovoltaics and are used as low-resistance contacts in organic light-emitting diodes and organic thin-film transistors. What makes metal oxides useful in these technologies is the fact that their chemical and electronic properties can be tuned to enable charge exchange with a wide variety of organic molecules. Although it is known that charge exchange relies on the alignment of donor and acceptor energy levels, the mechanism for level alignment remains under debate. Here, we conclusively establish the principle of energy alignment between oxides and molecules. We observe a universal energy-alignment trend for a set of transition-metal oxides—representing a broad diversity in electronic properties—with several organic semiconductors. The trend demonstrates that, despite the variance in their electronic properties, oxide energy alignment is governed by one driving force: electron-chemical-potential equilibration. Using a combination of simple thermodynamics, electrostatics and Fermi statistics we derive a mathematical relation that describes the alignment.**

Solar-energy conversion technologies based on organic semiconductors—such as dye-sensitized solar cells and organic photovoltaics[1–3]—as well as low-power-consumption electronic devices—such as organic light-emitting diodes[4–6] and organic thin-film transistors—use transition-metal oxides for efficient charge injection/collection between electrodes and organic molecules. The property that makes transition-metal oxides so useful to organic electronics is their ability to exchange charges with condensed molecules. This same property also allows certain oxides to photocatalytically convert $CO_2$ into useful hydrocarbons[7–9], and permits oxides to be used as electrolytes in solid-oxide fuel cells.

The ability of two materials to exchange charges requires the close alignment of donor and acceptor states in either material. A molecule's donor and acceptor states are its occupied and unoccupied frontier orbitals, respectively. When a molecule condenses onto a solid's surface, the molecule's frontier orbital energies change relative to their gas-phase values. The change of a molecule's frontier orbital energies when adsorbed to a surface can either enable or inhibit charge transfer with the solid.

An energy-level diagram of an oxide/organic interface is illustrated in Fig. 1a. The relevant parameters of energy-level alignment, such as oxide work function ($\phi$), highest occupied molecular orbital (HOMO) energy offset ($\Delta E_H$) and organic ionization energy ($IE_{org}$), are indicated in the figure[10]. Figure 1b,c shows how these parameters are extracted from ultraviolet photoemission spectroscopy (UPS) measurements.

Metal oxides were initially used in organic light-emitting diodes when it was discovered that some oxides have the ability to decrease the hole-injection barrier at anode/organic interfaces[11]. This discovery gave rise to decreased contact resistance in organic devices, resulting in vast improvements to device efficiency. This property is a result of oxides' ability to decrease the binding energy of an organic molecules' HOMO. It was later realized that some oxides exhibit a behaviour opposite to that of the hole-injecting materials[12], instead increasing the molecule's electron-orbital binding energies, thus lowering the lowest unoccupied molecular orbital (LUMO). These oxides can be used as electron-injecting materials.

Although both electron-injecting and hole-injecting transition-metal oxides are known, hole-injecting oxides are more common. Oxides such as $MoO_3$, $WO_3$, $V_2O_5$, CuO and NiO are known to be good hole-injection materials[6,13,14], whereas ones such as $TiO_2$ and $ZrO_2$ are better electron-injection materials[6,14,15]. Owing to their wide range of energy-aligning capabilities, metal oxides are now used in all types of organic electronic device. As transition-metal oxides exhibit such a large diversity in physical, chemical and electronic properties[16], they have great potential as materials that allow tuning of electron injection/extraction properties of electrodes.

To use these materials to their highest potential it is necessary to recognize those properties that most strongly affect energy-level alignment. However, the understanding of energy alignment at oxide/molecule interfaces is still inconclusive.

Over the past several decades a great deal of work has been devoted to understanding energy alignment in organic devices. Metal/organic interfaces were the first to be considered. Researchers initially assumed that vacuum levels would align at an interface[17]. Thus, they expected that the difference between a metal's work function and an organic molecule's HOMO and LUMO levels would determine charge-injection barriers. Researchers soon realized that vacuum levels rarely align[17], and it became uncertain what role work function plays in energy alignment.

Several developments to the interfacial energy alignment model arose, such as the interfacial pinning parameter[17,18], the concept of induced density of interface states[19,20], interfacial dipoles[21], the push-back/pillow effect[22], the importance of the charge-neutrality level[20,22] and the integer charge-transfer model[23,24]. These concepts reconcile some of the initial discrepancies in the energy-alignment model, but not all of these concepts are mutually consistent. Although many scientists and engineers routinely use work function as a 'back-of-the-envelope' evaluation of energy alignment, it is

[1]Department of Materials Science and Engineering, University of Toronto, 184 College St., Toronto, Ontario M5S 3E4, Canada, [2]Department of Physics, Yunnan University, 2 Cuihu Beilu, Yunnan, Kumming 650091, China. *e-mail: mark.greiner@utoronto.ca.

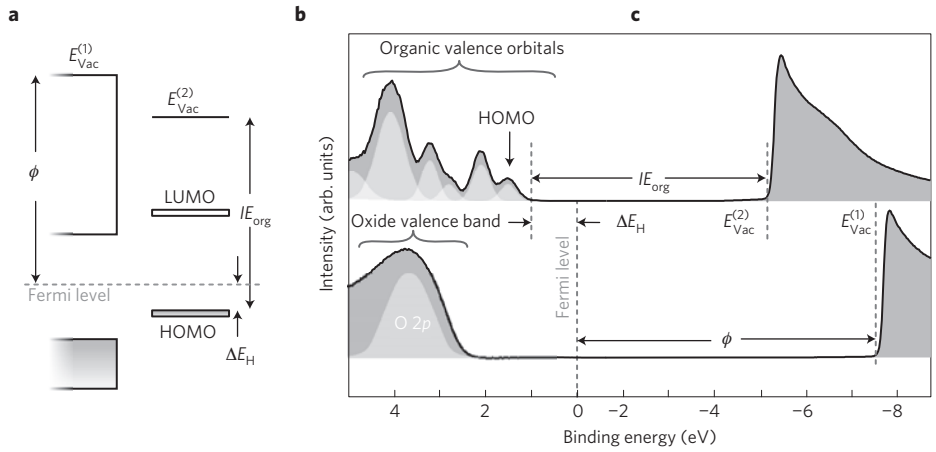


**Figure 1 | Energy levels at oxide/molecule interfaces. a**, Schematic energy-level diagram of an oxide/organic interface, with the substrate work function ($\phi$), vacuum level ($E_{vac}$), ionization energy ($IE$) and HOMO offset ($\Delta E_H$) indicated. **b**, Valence photoemission spectrum of 2T-NATA (top) and $MoO_3$ (bottom). **c**, Secondary electron spectrum of 2T-NATA (top) and $MoO_3$ (bottom). The arrows indicate how the parameters in **a** are determined from the spectra in **b** and **c**.

often taken for granted why this should be so. It is still uncertain how energy alignment is established, and a comprehensive and quantitative predictive model has not been developed.

When metal oxides became the topic of research, work function was seen to affect energy alignment only in the sense that it determines an oxide's valence- and conduction-band positions relative to the vacuum level. Many of the concepts developed for energy alignment at metal/organic interfaces do not necessarily hold for oxide/organic interfaces. For instance, most oxides do not have electron states at the Fermi level to enable charge exchange with molecules; thus, it is generally expected that charge transfer must proceed through an oxide's valence or conduction bands[25]. Indeed, several recent findings have shown convincing evidence that electrons can hop from an organic's HOMO level into the low-lying conduction bands of certain $d^0$ oxides, such as $MoO_3$ and $WO_3$ (refs 26–28). This has led many to believe that the energy-aligning characteristics of $MoO_3$ and $WO_3$ are a result of their low-lying conduction bands.

This charge-injection model is now frequently applied to a wide range of semiconductor/organic interfaces. However, this model is unable to explain why so many other oxides, having much different conduction- and valence-band positions than $MoO_3$ or $WO_3$, also work well as charge-injection layers. For example, NiO has a conduction band situated approximately 2 eV higher[29] than the HOMO level of α-NPD (*N*,*N*′-diphenyl-*N*,*N*′-bis(1-naphthyl)-1,1′-biphenyl-4,4′-diamine), but it still exhibits Ohmic hole-injection[30].

A global picture of oxide/organic energy alignment is not yet available. Although a Fermi-level-pinning transition was demonstrated previously[23], it was uncertain at the time whether this trend was actually universal, as it had been demonstrated using a limited set of *ex situ*-prepared samples. Here we demonstrate, using a large variety of *in situ*-prepared oxides, that such a Fermi-level-pinning transition is a universal trend, and is a result of an energy-alignment principle for non-reactive interfaces.

We have taken the approach of measuring a large set of diverse metal oxides because most present theories have been developed from small subsets of materials. The large variety of samples is very unique to this study, and illustrates the universality of the observed trend. The fact that this trend is observed for such diverse materials implies that substrate band structure does not affect the equilibrium energy-alignment position of adsorbed molecules. Rather, energy alignment is governed by the equilibration of a substrate's electron chemical potential with an adsorbed molecule's oxidation/reduction potentials. Using this concept, we present a simple mathematical formalism to predict energy alignment that is based on fundamental thermodynamic and electrostatic principles.

All samples were prepared *in situ* and characterized with core-level and valence-band photoemission spectroscopy. The oxides investigated here span a wide range of electronic properties, and include: n-type wide-bandgap semiconductors, such as $MoO_3$, $TiO_2$, $V_2O_5$, $WO_3$ and $Ta_2O_5$; defective semiconducting oxides, such as $MoO_{3-x}$, $TiO_{2-x}$, $V_2O_{5-x}$ and $CrO_{3-x}$; p-type semiconductors, such as $Cu_2O$, $Ag_2O$, $Cr_2O_3$ and $Co_3O_4$; p-type Mott–Hubbard insulators, such as CuO, NiO and CoO; and metallic oxides, such as $MoO_2$, $WO_2$ and TiO.

Three different organic semiconductors were paired with these oxides and their parent metals to identify broadly applicable trends in energy-level alignment. The organic semiconductors are: 4,4′,4″-tris(*N*-2-naphthyl-*N*-phenyl-amino)triphenylamine (2T-NATA); *N*,*N*′-diphenyl-*N*,*N*′-bis(1-naphthyl)-1,1′-biphenyl-4,4′-diamine (α-NPD); and 4,4′-bis(carbazol-9-yl)-2,2′-biphenyl (CBP).

Energy-level alignment was determined by measuring the HOMO levels of the three organic semiconductors (CBP, α-NPD and 2T-NATA), which were condensed into thin films on the above-mentioned oxides and the oxides' parent metals. Although numerous possible correlations were investigated—such as correlations between the organic HOMO energy and an oxide's valence-band position, conduction-band position and work function—the only relationship that was found to affect energy alignment was the energy difference between a substrate's work function and an organic's ionization energy.

The observed energy-alignment trend is shown in Fig. 2, where the HOMO offset ($\Delta E_H$) for molecular monolayers is plotted against substrate work function. The data for CBP (Fig. 2a), α-NPD (Fig. 2b) and 2T-NATA (Fig. 2c) are shown separately on the left. The data from separate molecules are combined into a universal plot in Fig. 2d by plotting HOMO offset against the difference of substrate work function and organic ionization energy. The dashed lines in Fig. 2d were determined by taking the average $\Delta E_H$ value for $\phi > IE$, and using linear regression for $\phi < IE$.

The trend in Fig. 2d shows a distinct change in energy alignment when a substrate's work function becomes equal to a molecule's ionization energy. Once a substrate's work function has exceeded an adsorbed molecule's ionization energy the HOMO offset establishes a minimum value, and remains constant with further increases in work function. This trend is similar to that observed for polymer-coated and *ex situ*-prepared substrates[23]. Here, using well-defined

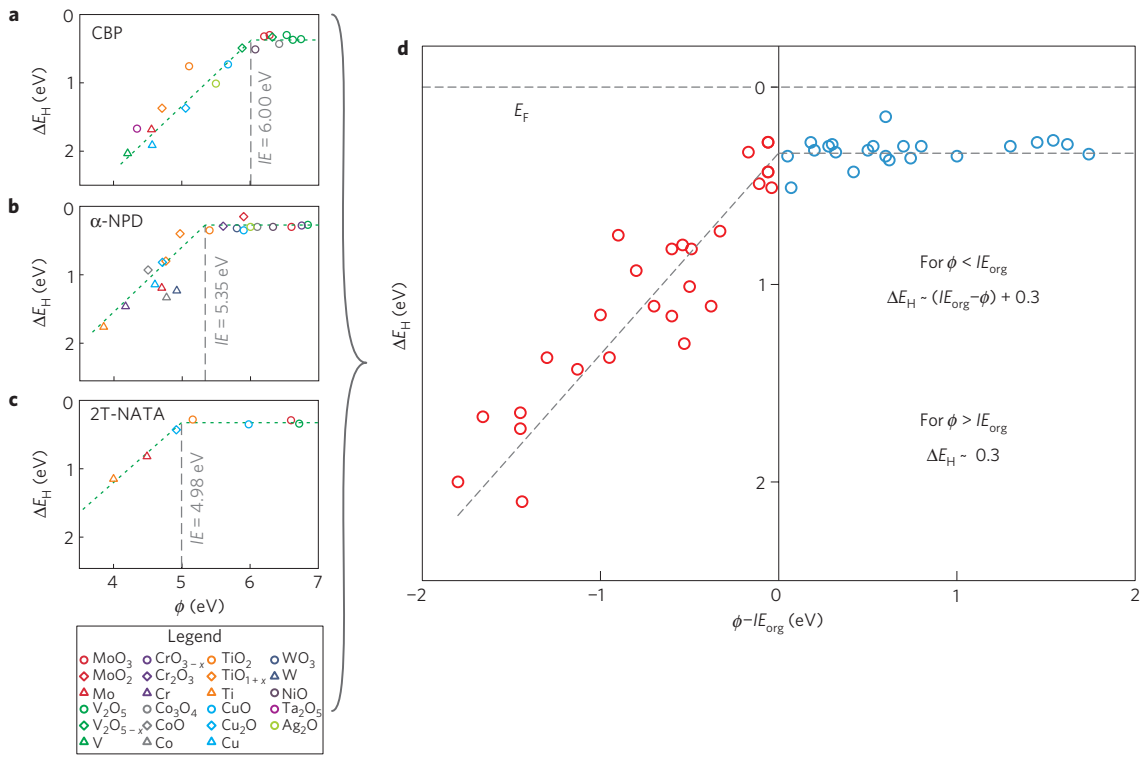


**Figure 2 | Universal energy-level alignment trends. a–c**, Plots of HOMO offset versus substrate work function for molecules CBP (**a**), α-NPD (**b**) and 2T-NATA (**c**) on various transition-metal oxide and transition-metal substrates (legend shown underneath). **d**, Universal plot of HOMO offset ($\Delta E_H$) versus the difference of substrate work function and organic ionization energy ($\phi - IE_{org}$) by combining plots **a–c**. The dashed line for $\phi > IE_{org}$ was determined by calculating the average $\Delta E_H$ value, and the dashed line for $\phi < IE_{org}$ was determined using a least-squares regression fit, with the restriction that $\Delta E_H = 0.3$ when $\phi = IE_{org}$.

oxides and metals prepared in ultrahigh vacuum, we find that this alignment principle is general and governs energy alignment of a wide range of materials.

Interestingly, as this trend is observed for a diverse set of materials it implies that the HOMO offset is independent of substrate electronic structure. To recognize the implications of this point it is important to review transition-metal oxide electronic structures. The main factor controlling their electronic structures is $d$-band occupancy[16]. In Fig. 3 we have divided the oxides into classes accordingly.

The left column in Fig. 3 presents each oxide class's schematic energy-level diagram, and the right column presents their valence-band photoemission spectra. For simplicity we describe the band structures using crystal field theory, using as a first approximation, the ionic model of bonding. In general, oxides have an energy gap in their $d$-bands from the non-spherical ionic coordination environments; however, for simplicity, we do not address the different cation coordination geometries and suffice to say that in general the $d$-bands have an energy gap.

The oxides with totally empty $d$-bands ($d^0$ oxides) constitute class 1. They are insulators in their stoichiometric forms, but tend to be n-type materials (that is, the Fermi level is close to the conduction band) owing to the presence of oxygen vacancy defects[16,31]. Their conduction-band minima are composed mainly of empty metal $d$-states, and valence-band maxima are composed primarily of O $2p$ states, as shown in Fig. 3ai.

A subset of class 1 oxides is the oxygen-deficient $d^0$ oxides. Oxygen deficiency generates a high density of occupied defect states close to the Fermi level, as illustrated in Fig. 3aii, making these oxides n-type semiconductors. The defect states arise from filling of empty metal $d$-states and can be seen in the valence spectra of Fig. 3bii.

The oxides whose $d$-bands are partially occupied with a low number of electrons (for example, $d^1$, $d^2$ and $d^3$) constitute class 2. These oxides tend to form when $d^0$ oxides are chemically reduced. They are often metallic, as illustrated by the band diagram in Fig. 3aiii and seen by the finite density of states at the Fermi level in the valence spectra level in Fig. 3biii.

The oxides whose $d$-bands are partially occupied with a high number of electrons (for example, $d^7$, $d^8$ and $d^9$) constitute class 3. These oxides tend to be Mott–Hubbard or charge-transfer insulators owing to strong electron correlation[32]. Their valence spectra show states that die off close to the Fermi level, as seen in Fig. 3biv.

Oxides with completely filled $d$-bands ($d^{10}$ oxides) constitute class 4. They tend to be semiconductors owing to the gap between the $d$-band and the next-highest energy band (usually derived from metal $s$-orbitals).

It is generally thought that, for an electron to jump from an organic molecule to an oxide, the electron must move from the organic's HOMO level into the oxide's conduction band, and thus an oxide's conduction-band positions should be very important for energy alignment. However, the pinning trend shown in Fig. 2 implies that energy alignment can be established regardless of oxide conduction/valence-band positions.

A compilation of oxide energy-level diagrams is shown in Fig. 4, along with energy-level diagrams of CBP, α-NPD and 2T-NATA. The band edges for the figure were determined from UPS spectra, and bandgaps were taken from literature values, which are tabulated and referenced in the Supplementary Information. The oxides are placed in order of decreasing work function (left to right) and the organics are placed in order of decreasing ionization energy (left to right).

A molecule's HOMO level can become pinned to the Fermi level even if the HOMO level is far away from the oxide's conduction

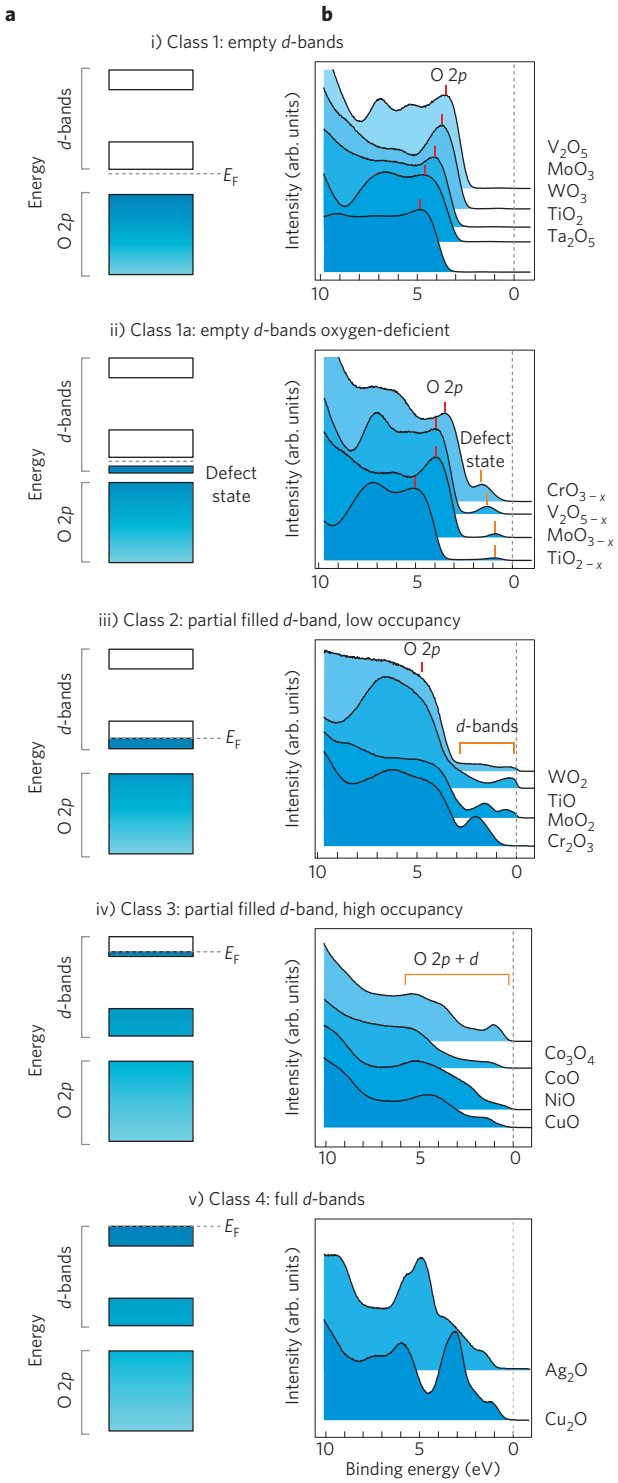


**Figure 3 | Valence bands of transition-metal oxide classes. a**, Schematic electron band diagrams of transition-metal oxides. **b**, Valence photoemission spectra of selected transition-metal oxides from each class. The classifications are based on the oxides' *d*-band occupancies, and are labelled from i to v.

or valence bands. For example, as shown in Fig. 4, α-NPD exhibits favourable energy alignment with numerous oxides—CuO, $Cr_2O_3$, $MoO_2$, $Co_3O_4$, NiO, $WO_3$, $V_2O_5$, $CrO_3$ and $MoO_3$—however, only $MoO_3$, $V_2O_5$, $WO_3$, $CrO_3$ and $MoO_2$ have conduction bands that are close enough to the HOMO level of α-NPD to permit thermal excitation of electrons into the oxides' conduction bands.

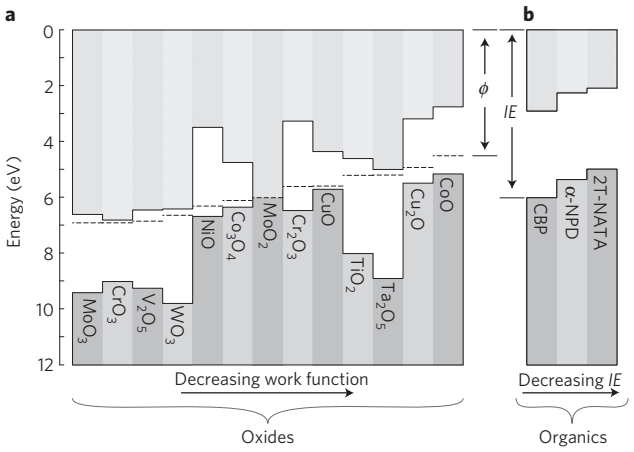


**Figure 4 | Energy levels of transition-metal oxides and organic semiconductors. a**,**b**, Compilation of valence and conduction bands for transition-metal oxides (**a**) and organic semiconductors (**b**) on an absolute energy scale (determined from direct and inverse photoemission, see Supplementary Information). Oxides are arranged in order of decreasing work function (from left to right) and organics are arranged in order of decreasing ionization energy (from left to right).

To understand why this occurs we have constructed an equation to describe the relationship between HOMO binding energy ($\Delta E_H$), substrate work function ($\phi$) and organic ionization energy ($IE_{org}$). The observed trend implies that HOMO level pinning occurs when the organic's ionization energy equals the substrate's Fermi energy, so we will consider how a charge particle is affected by the Fermi level. From solid-state and semiconductor physics, it is known that the formation energies of charged defects and ionized dopants depend on the Fermi level position[33,34]. As adsorbed molecules are in intimate contact with a solid, they are coupled to the solid's Fermi level, and so we will apply this concept to molecules adsorbed to a solid surface.

When an adsorbed neutral molecule becomes charged it gives (takes) an electron to (from) the Fermi level. Thus, its formation energy is given by the following equation.

$$E^f(M^q) = E(M^q) - E(M^0) - qE_F - E_{rlx}$$

Here, $E(M^q)$ is the total energy of a molecule carrying a charge of $q$, $E(M^0)$ is the energy of the neutral molecule, $E_F$ is the Fermi energy and $E_{rlx}$ is the relaxation energy, which depends on the screening characteristics of the surrounding substrate and molecules. Neglecting for the moment, relaxation effects, formation energy is simply the ionization energy for the $M^+$ state, plus an additional energy contribution from adding an electron to the solid's Fermi level. Thus, the Fermi energy has a direct influence on a charged molecule's thermodynamic stability.

Figure 5a shows a plot of the formation energy of molecules in the $M^0$ and $M^+$ states relative to the neutral molecule. When the Fermi energy becomes greater than the ionization energy of the molecule, the $M^+$ state becomes the thermodynamically favoured species. When the Fermi energy lies within the energy gap of the molecule the neutral state is most stable.

The band diagrams of two hypothetical oxides with different work functions are shown to the right of the formation energy plot in Fig. 5a. Oxide 1, having the lower work function, has a Fermi level that sits above the point of transition from $M^0 \rightarrow M^+$. When adsorbed to the surface of oxide 1 the neutral molecule is most stable. As oxide 2 has a higher work function, such that its Fermi level sits below the point of transition from $M^0 \rightarrow M^+$, the ionized molecule is the most stable form when adsorbed to oxide 2.

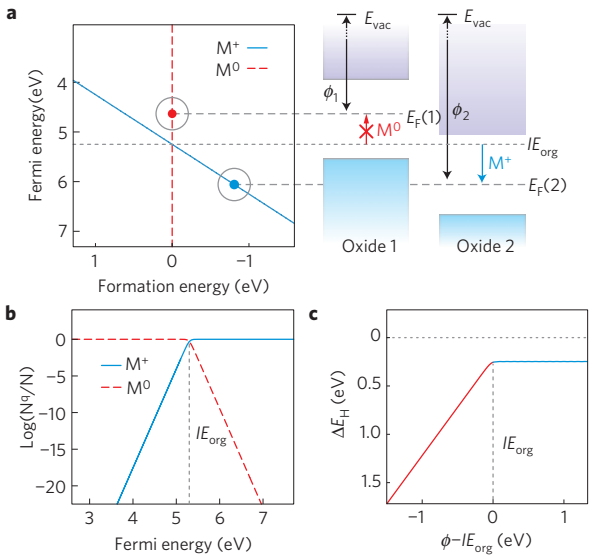


**Figure 5 | Origin of energy-level-alignment trend. a**, Formation energies of adsorbed molecular species $M^0$ and $M^+$ as a function of the substrate Fermi energy. The points on the formation energy plot correspond to two hypothetical oxides with band structures as shown to the right. **b**, Plot showing how the relative concentrations ($N^q/N$) of molecular species $M^0$ and $M^+$ in a monolayer change with the substrate's Fermi level. **c**, Plot of HOMO offset ($\Delta E_H$) versus the difference between substrate work function and organic ionization energy ($\phi - IE_{org}$) calculated from equation (2).

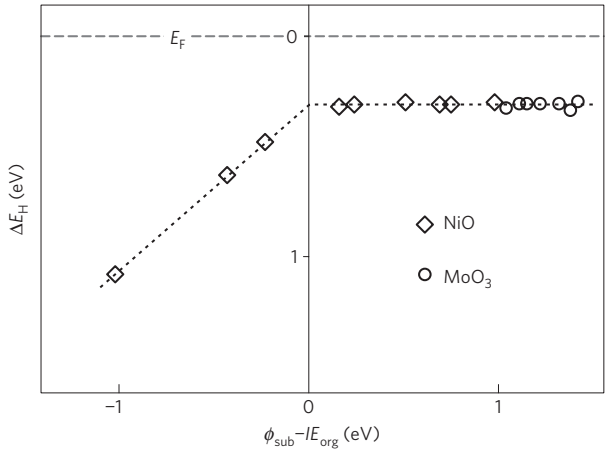


**Figure 6 | Tuning energy alignment through electron chemical potential.** Plot of HOMO offset ($\Delta E_H$) versus the difference between substrate work function and organic ionization energy ($\phi - IE_{org}$) for α-NPD on NiO and $MoO_3$, where the electron chemical potential of the oxides was tuned by inducing oxygen vacancy defects.

When a solid's Fermi level falls below a molecule's ionization energy, the number of ionized molecules rapidly increases. As the charged molecule's stability is coupled to the Fermi level, Fermi–Dirac statistics must be used in calculating the equilibrium concentrations of charged molecules[34]. Their relative concentrations are given by equation (1).

$$\frac{N^q}{N} = \left(1 + g(M^q)\exp\left[\frac{E^f(M^q)}{kT}\right]\right)^{-1} \quad (1)$$

where $N^q$ is the number of molecules of charge $q$ in the first monolayer adsorbed to the surface. $N$ is the total number of molecules in the first layer, $g(M^q)$ is a degeneracy factor, which accounts for the number of identical charged configurations of a molecule, and $E^f(M^q)$ is the formation energy of a molecule with a charge of $q$. The logarithm of the relative concentrations of each molecular species (equation (1)) is plotted in Fig. 5b.

To model energy alignment we must consider how charged molecules affect the electric field at the interface. When the Fermi energy lies within the molecule's HOMO–LUMO gap, essentially all of the adsorbed molecules are neutral; thus, they do not generate an electric field and cannot counteract the Volta potential at the substrate surface (see Supplementary Information for more details of how a Volta potential arises at the substrate surface). As the Volta potential increases linearly with substrate work function the HOMO binding energy shifts linearly with substrate work function.

As the Fermi energy moves below the adsorbed molecule's ionization energy, the equilibrium concentration of ionized molecules rapidly increases. The presence of positively charged molecules generates a positive electric field in the organic layer, which counteracts the negative electric field from the substrate's surface potential. As the work function increases further, the concentration of ionized molecules increases, such that the electric field and HOMO energy remain constant with increasing work function.

This scenario can be modelled by treating the adsorbed ionized molecules as a charged plane, where the charge on the plane depends on the concentration of ionized molecules in the plane. We can write an equation that calculates the HOMO offset as a function of ionization energy and substrate work function.

$$E_H = IE - \alpha\phi + \delta + \frac{q^2\rho d}{2\epsilon_0}\sum_{i=0}^{\infty}\left(1 + g\exp\left[\frac{IE - (\phi - i\beta)}{kT}\right]\right)^{-1} \quad (2)$$

where $IE$ is the molecule's ionization energy, $\delta$ is the interfacial dipole from the 'push-back' effect, $\alpha$ is a proportionality constant based on the molecular layer's ability to screen the potential of the substrate surface, $\phi$ is the substrate's work function, $q$ is the elementary charge, $\rho$ is the planar number density of molecules and $d$ is the distance between the molecular plane and the substrate. The summation is taken over $i$ molecular layers. Equation (2) is plotted in Fig. 5c, where one can see that it reproduces the observed relationship between HOMO offset and substrate work function.

The above model implies that pinning occurs because, when a molecule is adsorbed to a surface and coupled with the solid's Fermi energy, the ionized form of the molecule becomes thermodynamically stable when the Fermi energy is greater than the molecule's ionization energy. This implies that oxide band structure does not govern energy alignment because it does not govern the thermodynamic stability of charged molecules. Conduction bands and valence bands simply provide a convenient pathway for conduction, but the pathway for reaching equilibrium need not be well defined for equilibrium to ultimately be reached.

Although changing materials is one method of altering an electrode's chemical potential, an oxide's chemical potential can also be tuned by introducing oxygen defects. By removing oxygen atoms an oxide's electron chemical potential can be decreased. Oxygen vacancies act as n-type dopants and raise the Fermi level, thus reducing the work function. Conversely, oxygen interstitials can increase the oxide's electron chemical potential. This principle can be used to tune the energy alignment of an oxide.

To illustrate this point, we have taken two oxides (NiO and $MoO_3$) and tuned their electron chemical potentials by inducing defects, then examined how the energy alignment of α-NPD is affected, as shown in Fig. 6. NiO is known to form oxygen interstitial defects, whereas $MoO_3$ is known to form oxygen vacancy defects. The work function of NiO can be increased by growing the oxide under more oxidative conditions, such as higher temperatures, higher oxygen pressures or by using $O_3$ for oxidation. As shown in Fig. 6, when the work function of NiO increases the HOMO offset

of α-NPD decreases until its ionization energy is reached and the HOMO level becomes pinned.

On the other hand, the work function of $MoO_3$ can be decreased by annealing in vacuum. $MoO_3$ has such a high work function that even a defective oxide has a work function greater than the ionization energy of α-NPD. Thus, the HOMO binding energy of α-NPD stays pinned to the Fermi level of $MoO_3$ over the whole range of work functions exhibited by $MoO_3$.

Therefore, if electron chemical potential is the driving force for energy-level alignment, what makes transition-metal oxides so special? Oxides simply modify the surface potential of a substrate; however, metal oxides are capable of a wide range of work functions from $\sim 2$ eV ($ZrO_2$) to $\sim 7$ eV ($V_2O_5$). They can be made to position molecular levels close to the Fermi level for most organic semiconductors to enable efficient charge transfer. Their work functions and electronic structures can be tuned by inducing defects or changing the oxidation state of the metal cation. This versatility gives oxides a broad range of applications in organic electronics, as well as in heterogeneous catalysis.

## Methods

Photoemission measurements were conducted on a PHI 5500 Multitechnique system using a monochromated Al Kα photon source ($h\nu = 1{,}486.7$ eV) for X-ray photoemission spectroscopy (XPS) and a non-monochromated He Iα photon source ($h\nu = 21.22$ eV) for UPS. Oxide stoichiometries and oxidation states were identified using high-resolution core-level XPS (see Supplementary Information for spectra). Work function and valence-band measurements were carried out using UPS with the sample tilted to a take-off angle of 90° and under an applied bias of −15 V. The analysis chamber base pressure was $\sim 10^{-10}$ torr. Further details are available in the Supplementary Information.

Oxides were prepared by *in situ* oxidation of metal films. The metal films were ~200 nm thick, deposited onto polished silicon wafers by radiofrequency sputter deposition of pure (>99.99%) metal targets. Metal substrates were nanocrystalline, with an average grain size of 30 nm and an r.m.s. roughness of ~1 nm, as measured with atomic force microscopy. Substrates did not exhibit observable roughening after oxidation.

Organic films were deposited, in an attached vacuum chamber with a base pressure better than $10^{-9}$ torr, using sublimation-purified molecular organic powders in Knudsen cells. Film thickness was determined using a calibrated oscillating quartz monitor. Work function and HOMO binding energy profiles were determined using the layer-by-layer UPS technique (described in the Supplementary Information). Experimental validation was carried out to ensure radiation damage was not causing spurious correlations (see Supplementary Information for more details).

Received 9 June 2011; accepted 4 October 2011; published online 6 November 2011; corrected online 1 December 2011 and 6 December 2011

## References


1. O'Regan, B. & Grätzel, M. A low-cost, high-efficiency solar-cell based on dye-sensitized colloidal $TiO_2$ films. *Nature* **353,** 737–740 (1991).
2. Gibson, E. A. *et al.* A p-type NiO-based dye-sensitized solar cell with an open-circuit voltage of 0.35 V. *Angew. Chem. Int. Ed.* **48,** 4402–4405 (2009).
3. Nattestad, A. *et al.* Highly efficient photocathodes for dye-sensitized tandem solar cells. *Nature Mater.* **9,** 31–35 (2010).
4. Kabra, D., Lu, L. P., Song, M. H., Snaith, H. J. & Friend, R. H. Efficient single-layer polymer light-emitting diodes. *Adv. Mater.* **22,** 3194–3198 (2010).
5. Meyer, J., Khalandovsky, R., Gorrn, P. & Kahn, A. $MoO_3$ films spin-coated from a nanoparticle suspension for efficient hole-injection in organic electronics. *Adv. Mater.* **23,** 70–73 (2011).
6. Qiu, C. F., Xie, Z. L., Chen, H. Y., Wong, M. & Kwok, H. S. Comparative study of metal or oxide capped indium-tin oxide anodes for organic light-emitting diodes. *J. Appl. Phys.* **93,** 3253–3258 (2003).
7. Roy, S. C., Varghese, O. K., Paulose, M. & Grimes, C. A. Toward solar fuels: Photocatalytic conversion of carbon dioxide to hydrocarbons. *ACS Nano* **4,** 1259–1278 (2010).
8. Chueh, W. C. *et al.* High-flux solar-driven thermochemical dissociation of $CO_2$ and $H_2O$ using nonstoichiometric ceria. *Science* **330,** 1797–1801 (2010).
9. Varghese, O. K., Paulose, M., LaTempa, T. J. & Grimes, C. A. High-rate solar photocatalytic conversion of $CO_2$ and water vapor to hydrocarbon fuels. *Nano Lett.* **9,** 731–737 (2009).
10. Ishii, H., Sugiyama, K., Ito, E. & Seki, K. Energy level alignment and interfacial electronic structures at organic/metal and organic/organic interfaces. *Adv. Mater.* **11,** 605–625 (1999).
11. Tokito, S., Noda, K. & Taga, Y. Metal oxides as a hole-injecting layer for an organic electroluminescent device. *J. Phys. D* **29,** 2750–2753 (1996).
12. Tang, H., Li, F. & Shinar, J. Bright high efficiency blue organic light-emitting diodes with $Al_2O_3$/Al cathodes. *Appl. Phys. Lett.* **71,** 2560–2562 (1997).
13. Chu, C. W., Li, S. H., Chen, C. W., Shrotriya, V. & Yang, Y. High-performance organic thin-film transistors with metal oxide/metal bilayer electrode. *Appl. Phys. Lett.* **87,** 193508 (2005).
14. Wang, Z. B., Helander, M. G., Greiner, M. T., Qiu, J. & Lu, Z. H. Analysis of charge-injection characteristics at electrode-organic interfaces: Case study of transition-metal oxides. *Phys. Rev. B* **80,** 235325 (2009).
15. Murdoch, G. B., Greiner, M., Helander, M. G., Wang, Z. B. & Lu, Z. H. A comparison of CuO and $Cu_2O$ hole-injection layers for low voltage organic devices. *Appl. Phys. Lett.* **93,** 083309 (2008).
16. Henrich, V. E. & Cox, P. A. *The Surface Science of Metal Oxides* (Cambridge Univ. Press, 1996).
17. Ishii, H. & Seki, K. Energy level alignment at organic/metal interfaces studied by UV photoemission: Breakdown of traditional assumption of a common vacuum level at the interface. *IEEE Trans. Electron Devices* **44,** 1295–1301 (1997).
18. Hill, I. G., Rajagopal, A., Kahn, A. & Hu, Y. Molecular level alignment at organic semiconductor–metal interfaces. *Appl. Phys. Lett.* **73,** 662–664 (1998).
19. Vazquez, H., Flores, F. & Kahn, A. Induced density of states model for weakly-interacting organic semiconductor interfaces. *Org. Electron.* **8,** 241–248 (2007).
20. Vazquez, H., Gao, W., Flores, F. & Kahn, A. Energy level alignment at organic heterojunctions: Role of the charge neutrality level. *Phys. Rev. B* **71,** 041306 (2005).
21. Crispin, X. *et al.* Characterization of the interface dipole at organic/metal interfaces. *J. Am. Chem. Soc.* **124,** 8131–8141 (2002).
22. Vázquez, H., Dappe, Y. J., Ortega, J. & Flores, F. Energy level alignment at metal/organic semiconductor interfaces: Pillow effect, induced density of interface states, and charge neutrality level. *J. Chem. Phys.* **126,** 144703 (2007).
23. Tengstedt, C. *et al.* Fermi-level pinning at conjugated polymer interfaces. *Appl. Phys. Lett.* **88,** 053502 (2006).
24. Braun, S., Salaneck, W. R. & Fahlman, M. Energy-level alignment at organic/metal and organic/organic interfaces. *Adv. Mater.* **21,** 1450–1472 (2009).
25. Sessolo, M. & Bolink, H. J. Hybrid organic–inorganic light-emitting diodes. *Adv. Mater.* **23,** 1829–1845 (2011).
26. Kroger, M. *et al.* Role of the deep-lying electronic states of $MoO_3$ in the enhancement of hole-injection in organic thin films. *Appl. Phys. Lett.* **95,** 123301 (2009).
27. Sessolo, M. H. B. Hybrid organic–inorganic light emitting diodes. *Adv. Mater.* **23,** 1829–1845 (2011).
28. Lee, H. *et al.* The origin of the hole injection improvements at indium tin oxide/molybdenum trioxide/N, N′-bis(1-naphthyl)-N, N′-diphenyl-1, 1′-biphenyl- 4, 4′-diamine interfaces. *Appl. Phys. Lett.* **93,** 043308 (2008).
29. Zimmermann, R. *et al.* Electronic structure of 3d-transition-metal oxides: on-site Coulomb repulsion versus covalency. *J. Phys.:Condes. Matter.* **11,** 1657–1682 (1999).
30. Kanno, H., Sun, Y. & Forrest, S. R. High-efficiency top-emissive white-light-emitting organic electrophosphorescent devices. *Appl. Phys. Lett.* **86,** 263502 (2005).
31. Scanlon, D. O., Walsh, A., Morgan, B. J. & Watson, G. W. An *ab initio* study of reduction of $V_2O_5$ through the formation of oxygen vacancies and Li intercalation. *J. Phys. Chem. C* **112,** 9903–9911 (2008).
32. Hüfner, S. Electronic structure of NiO and related 3d-transition-metal compounds. *Adv. Phys.* **43,** 183–356 (1994).
33. Van de Walle, C. G. & Neugebauer, J. Universal alignment of hydrogen levels in semiconductors, insulators and solutions. *Nature* **423,** 626–628 (2003).
34. Sze, S. M. *Physics of Semiconductor Devices* 2 edn (Wiley, 1981).


## Acknowledgements

We thank J. Nogami, C. Mims and G. Walker for their helpful advice. We also thank D. Grozea for his technical assistance, and E. Nolan for his help editing the manuscript. We would also like to thank R. D'Souza-Greiner for proofreading the manuscript. The financial support for this research was provided by the NRC-NSERC-BDC Nanotechnology Initiative (NNBPJ364261-07). Z-H.L. is the Canada Research Chair in Organic Optoelectronics, Tier I.

## Author contributions

M.T.G. planned the study, carried out XPS and UPS measurements and wrote the manuscript. M.G.H. assisted in XPS and UPS experiments, as well as method validation, and participated in discussion. W-M.T. prepared samples and assisted with atomic force microscopy measurements. Z-B.W. and J.Q. took part in discussion and assisted in sample preparation. Z-H.L. supervised the research, and gave direction in writing the manuscript.

## Additional information

The authors declare no competing financial interests. Supplementary information accompanies this paper on www.nature.com/naturematerials. Reprints and permissions information is available online at http://www.nature.com/reprints. Correspondence and requests for materials should be addressed to M.T.G.

CORRIGENDUM

# Universal energy-level alignment of molecules on metal oxides

Mark T. Greiner, Michael G. Helander, Wing-Man Tang, Zhi-Bin Wang, Jacky Qiu and Zheng-Hong Lu

*Nature Materials* http://dx.doi.org/10.1038/nmat3159 (2011); published online 6 November 2011; corrected online 1 December 2011 and 6 December 2011.

In the version of this Article originally published online, equation (2) was incorrect and the parameter definitions incomplete. These errors have been corrected in all versions of the Article.